

Progress in Nuclear Energy
Manuscript Draft

Manuscript Number: PNUCENE-D-14-00301

Title: CFD study of an air-water flow inside helically coiled pipes

Article Type: Research Paper

Keywords: Eulerian multiphase model; CFD; Helical coil; Air-water flow

CFD study of an air-water flow inside helically coiled pipes

Marco Colombo^{a,b}, Antonio Cammi^{*a}, Gael Guedon^a, Fabio Inzoli^a

^aDepartment of Energy, Politecnico di Milano, Via Lambruschini 4, 20156, Milano, Italy

^bPresent address: Institute of Particle Science and Engineering, School of Process, Material and Environmental Engineering, University of Leeds, Leeds LS2 9JT, United Kingdom

*Corresponding author

Tel.: +39 02 2399 6332

Fax: +39 02 2399 8566

Email: antonio.cammi@polimi.it

Abstract

CFD is used to study an air-water mixture flowing inside helically coiled pipes, being at the moment considered for the Steam Generators (SGs) of different nuclear reactor projects of Generation III+ and Generation IV.

The two-phase mixture is described through the Eulerian-Eulerian model and the adiabatic flow is simulated through the ANSYS FLUENT code. A twofold objective is pursued. On the one hand, obtaining an accurate estimation of important physical quantities, as the frictional pressure drop and the void fraction, which are particularly important for the design. In this perspective, CFD simulations can provide accurate predictions without being limited to a particular range of system parameters, which often constricts the application of empirical correlations. On the other hand, a better understanding of the role of the centrifugal force field is pursued, being required to improve the knowledge of the component behavior and assure a more efficient and safe operation of the nuclear plant.

The effect of the centrifugal force field introduced by the geometry is characterized and qualitatively compared with experimental observations. Water is pushed by the centrifugal force towards the outer pipe wall, whereas air accumulates in the inner region of the pipe. The maximum of the mixture velocity is therefore shifted towards the inner pipe wall, as the air flows much faster than the water, having a considerably lower density. The flow field, as for the single-phase flow, is characterized by flow recirculation and vortices. Quantitatively, the simulation results are assessed with the experimental data of Akagawa et al. (1971) for void fraction and frictional pressure drop. The use of a relatively simple model of momentum interfacial transfers allows obtaining a very good agreement for the void fraction and a satisfactory estimation of the frictional pressure drop. Effects on results of changes in the diameter of the dispersed phase are described, as its value strongly affects the degree of interaction between the phases. In addition, a more precise treatment of the near wall region other than wall function results in a better definition of the liquid film at the wall, although an overestimation of the frictional pressure drop is obtained.

KEYWORDS: Helical pipes; CFD study; Eulerian multiphase model; Frictional pressure drop; Void fraction; Experimental data.

1. Introduction

Different nuclear reactor projects of Generation III+ and Generation IV are expected to adopt helically coiled pipes in their Steam Generators (SGs). Helical pipes provide a substantial improvement in heat and mass transfer rates and a significant enhancement of the critical heat flux during boiling and evaporation. To the higher heat transfer rates contributes the geometrical arrangement, which combines the positive features of a local cross-flow distribution with the global counter-flow along the exchanger tube (Bejan and Kraus, 2003). Helical geometry allows also handling of high temperatures and extreme temperature differentials without high induced stresses. In addition, helical pipes guarantee a compact design of the SG, reducing the required floor space (Cinotti et al., 2002). The above features improve the general efficiency of the SG, moving forward towards the goals of improved safety, performance and cost established by the nuclear community for future reactor projects.

Helical tubes are normally used in different industrial fields (Naphon and Wongwises, 2006). They have been previously adopted for the SG of more than one nuclear reactor, although mainly for prototypes or special applications. Nevertheless, issues still exist in the understanding of some complex thermal hydraulic mechanisms activated by the centrifugal force field introduced by the geometry. Obviously, the complexity is further amplified by the presence of a two-phase flow. In the past, the lack of a full understanding has been solved with the adoption of conservative safety limits, that guarantee safety operation despite limiting the optimal exploitation of the plant. Nowadays, overcome those limitations is made possible by the more and more powerful computational resources available for the optimization of the design and the improvement of the safety evaluations (Bousbia-Salah and D'Auria, 2007).

Recently, two-phase Computational Fluid Dynamics (CFD) has been increasingly applied in the nuclear field, as a promising way to extend simulation capabilities of many nuclear reactor thermal hydraulic issues. A Writing Group of the OECD-NEA has identified a list of nuclear reactor safety issues in which the use of two-phase CFD can provide a real benefit. Moreover, the various modeling options were identified and some first Best Practice Guidelines has been proposed (Bestion, 2012). In particular, promising is the coupling of CFD codes to best estimate system codes, adopted for safety analysis and transient thermal hydraulic calculations, as RELAP5 or TRACE (Aumiller et al., 2002; Bertolotto et al., 2009). The coupling between the codes limits the application of the more computationally expensive CFD to those areas where three dimensional flow effects and mixing phenomena are important, avoiding at the same time the modeling of the entire geometry (Anderson et al., 2008).

Two-phase CFD offers great potential to the study of helical pipes, being three dimensional flow effects significant for the presence of the secondary motion introduced by the geometry. However, publications available on the subject are rather limited. (Vashisth and Nigam (2009) simulated laminar two-phase flow in coiled ducts using the Volume of Fluid (VOF) model to study the radial asymmetry of the velocity field. A good agreement with literature experimental data is obtained.) Jo et al. (2009) investigated the two-phase flow heat transfer in the helical tubes of a pressurised water reactor SG using the CFX code. They reported the formation of a liquid film on the outer portion of the tube and a good agreement with experimental data. Jajakumar et al. (2010) presented a CFD analysis for the heat transfer of an air-water two-phase mixture flowing through a helically coiled heat exchanger, identifying the effect of different geometrical parameters. Rahimi et al. (2011)

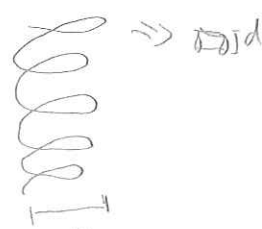
studied an air-water two-phase flow with CFD and population balance modeling (PBM) for bubble size distribution, which resulted more appropriate to capture the main flow features. Chandratilleke et al. (2012) studied flow boiling in curved pipes with a non-equilibrium model based on the Eulerian-Eulerian approach, obtaining a satisfactory agreement with experiments.

In this paper, CFD is applied to the simulation of the two-phase flow inside an helically coiled duct. The capability of an accurate quantitative estimation of important physical quantities as the frictional pressure drop and the void fraction is evaluated, being particularly important in the design process. At the same time, a better understanding of some basic physical phenomena is pursued (e.g., the effect of the centrifugal force field), requiring a high level of detail in the results. The latter in particular is important for a complete knowledge of the component operation, required to assure a more efficient and safer operation of the nuclear plant. The ANSYS FLUENT (2011) code is selected for the simulations, with the air-water flow described through the Eulerian-Eulerian model. The fundamental step for a confident utilization of the numerical model is the assessment of its accuracy with experimental data. With the aim to extend the analysis to a steam-water flow in the near future, the analysis is started with the air-water flow for the larger availability of the experimental data required for validation. Actually, for an important parameter as the void fraction, experimental data are limited to the air-water case. In particular, the simulation results are compared with experimental data of frictional pressure drop and void fraction from the work of Akagawa et al. (1971). In addition, a qualitative assessment of the phase distribution is proposed with some experimental observations obtained with imaging tomography (Murai, 2005). Through comparison with experiments, the capability of the model to characterize the two-phase flow inside the pipe and predict the frictional pressure drop and the void fraction are evaluated. Usually, these quantities are evaluated with empirical correlations, which are often unavoidably related to the experimental database used for their development. On the contrary, CFD could be capable of a high accuracy without being limited to a particular geometry or a narrow range of operating conditions.

2. Experimental data

A comprehensive research on air-water two-phase flow inside helically coiled pipes was published by Akagawa et al. (1971). In the paper, the authors study through experiments the flow pattern, the void fraction and the frictional pressure drop. Two different helices were used, with the same tube diameter d equal to 9.93 mm and coil diameter of 0.109 m and 0.225 m, for a d/D ratio respectively of 0.091 and 0.044. The water superficial velocity ranges between 0.35 m/s and 1.16 m/s, while the gas superficial velocity within 0 m/s and 5 m/s. In particular, for each one of the four fixed values of the liquid flow rate, the air flow rate is gradually increased starting from a very low value. The void fraction measurements are shown in Figure 1. The frictional pressure drop data are shown for both coils in Figure 2, where the four liquid superficial velocities are distinguished. In this paper, three sets of data from Akagawa et al. were considered for the assessment of the numerical results, at $j_w = 0.85$ m/s and 1.16 m/s for the 0.109 m diameter coil and at $j_w = 0.35$ m/s for the 0.225 m diameter coil.

Why?
What are the criteria
for choosing this set of data?



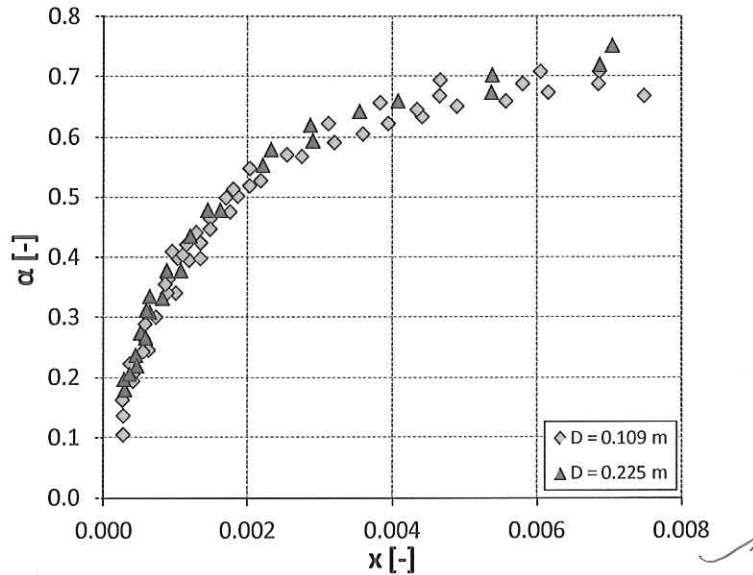


Figure 1 Void fraction experimental data from the work of Akagawa et al. (1971). The data are related to both the helices tested by the authors (coil diameter $D = 0.109$ m and $D = 0.225$ m respectively).

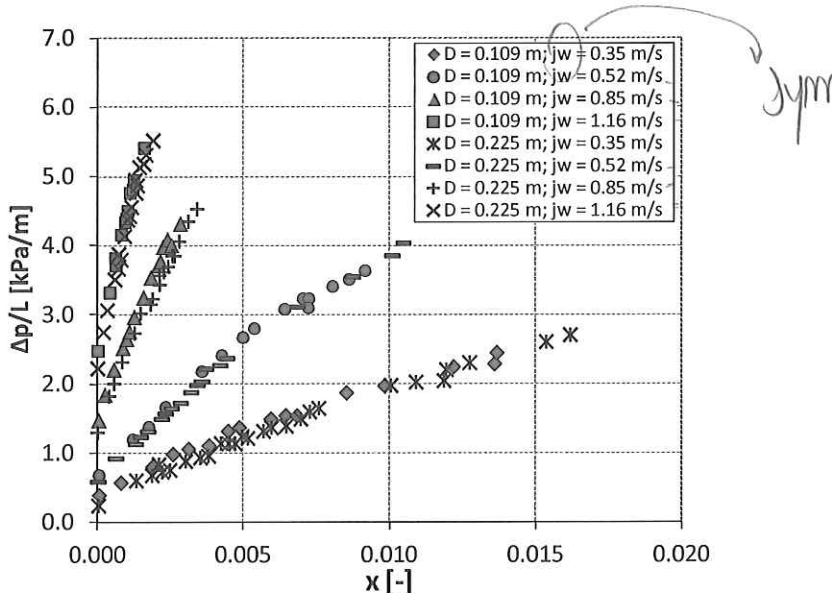


Figure 2 Frictional pressure drop experimental data from the work of Akagawa et al. (1971). The data are related to both the helices tested by the authors (coil diameter $D = 0.109$ m and $D = 0.225$ m respectively).

3. Numerical model

Numerical simulations were performed with the ANSYS FLUENT 14.0 (2011) code. The description of a multiphase flow is a very complex subject, as the distribution of the two phases changes continuously and in a random fashion. The presence of the interface and the resulting exchanges of mass, momentum and energy between the phases complicate enormously the analysis, since the shape of the interface is predictable only in a very restricted number of cases. In addition,

since the interfacial exchanges take place in a dynamic way, multiphase flows are often not in thermal and velocity equilibrium, so that the two phases flow with different temperatures and velocities.

Between the approaches available to describe multiphase flows, the Eulerian-Eulerian model has been preferred. The Eulerian-Eulerian model describes the two phases as interpenetrating continua, where the conservation equations for each phase are based on an averaging procedure that allows both phases to co-exist at any point. Since space and time averaging are applied, all the information regarding position and shape of the interface are lost. Only statistical or averaged information are available through quantities as the void fraction, which quantifies in any point the relative weight between the phases. Being lost the detailed topology of the phases, the interfacial mass, momentum and energy exchanges need to be explicitly modeled to close the system of equations. However, with respect to other methods which track the interface position and solve interfacial phenomena and deformations to the smallest length scales without filtering (e.g., VOF), the Eulerian-Eulerian model allows to preserve a large amount of computational time. In addition, in many practical situations or technological contexts there is more interest in some averaged quantities rather than in the detailed knowledge of the motion of all the particles or of the interstitial fluid. Therefore, it might be advantageous to compute directly the time evolution of these averaged quantities (Prosperetti and Tryggvasson, 2007).

The adiabatic air-water mixture is simulated neglecting the phase change and the heat transfer between the phases. Therefore, the two fluids are in thermal equilibrium. The fluid properties are also considered constant and their values can be found in Table 1.

Table 1 Fluid properties used in the simulation of the air-water mixture.

ρ_w [kg/m ³]	998.2
μ_w [Pa·s]	1.225
ρ_a [kg/m ³]	0.001
μ_a [Pa·s]	$1.79 \cdot 10^{-5}$
σ [N/m]	0.0727

In the momentum equation, the momentum transfer between the phases is taken into account only by the drag force, whereas all the other interfacial forces are neglected. Therefore, the following set of conservation equations are solved for each phase (ANSYS FLUENT, 2011):

$$\frac{\partial}{\partial t}(\alpha_k \rho_k) + \nabla \cdot (\alpha_k \rho_k \mathbf{v}_k) = 0 \quad (1)$$

$$\frac{\partial}{\partial t}(\alpha_k \rho_k \mathbf{v}_k) + \nabla \cdot (\alpha_k \rho_k \mathbf{v}_k \mathbf{v}_k) = -\alpha_k \nabla p + \nabla \cdot \mathbf{T}_k + \alpha_k \rho_k \mathbf{g} + \sum_{p=1}^2 \mathbf{R}_{pk} \quad (2)$$

Considering the equation for phase 1, the interaction term between the phases R_{ph} assumes the following form:

$$\mathbf{R}_{21} = K_{21} \cdot (\mathbf{v}_2 - \mathbf{v}_1) \quad (3)$$

For the calculation of the interaction term, the model assumes the secondary phase to always form droplets or bubbles. If phase 1 represents the continuous phase, while phase 2 the dispersed phase, the exchange coefficient K is written in the following form:

$$K_{21} = \frac{\alpha \cdot (1-\alpha) \rho_2 f}{\tau_2} \quad (4)$$

The term τ_2 represents the “particulate relaxation time”, which reads:

$$\tau_2 = \frac{\rho_2 d_p^2}{18 \mu_1} \quad (5)$$

Particularly important is the diameter of the bubbles or droplets of the dispersed phase d_p , that will be further addressed in the following sections. In Eq. (4), f is the drag function, calculated using the universal drag law (Kolev, 2005):

$$f = \frac{C_D Re}{24} \quad (6)$$

The drag coefficient C_D is a function of the type of two-phase flow and the flow regime. Re is the local relative velocity Reynolds number:

$$Re = \frac{\rho_1 \cdot (\mathbf{v}_1 - \mathbf{v}_2) d_p}{\mu_e} \quad (7)$$

The viscosity μ_e , is an effective viscosity accounting for the effects of the discrete phase on the continuum phase. The $k-\epsilon$ turbulence model has been used to simulate turbulence, with the standard wall function for the treatment of the near wall region (ANSYS FLUENT, 2011). An analysis using the enhanced wall treatment is also presented. In this case, the near wall region is completely resolved all the way to the viscous sub layer. The pressure-velocity coupling is resolved using the Phase Coupled SIMPLE algorithm (ANSYS FLUENT, 2011), extension of the SIMPLE algorithm to multiphase flow (Patankar, 1980). Momentum and turbulent quantities are discretised with the second order upwind scheme, while the QUICK scheme is used for the void fraction. A convergence criterion of 10^{-5} is applied for velocities, volume fraction and turbulent quantities. The no slip condition is applied at the tube wall, together with a constant outlet pressure boundary condition.

Time dependent simulations assure a proper convergence of the results. The following procedure has been adopted. For every simulated condition, initially a first calculation was made with a coarser grid, to reach a developed flow condition. A homogeneous mixture is considered as the inlet boundary condition. Outlet velocity and void fraction profiles from the first simulation are then applied as inlet conditions in successive simulations, to obtain the final simulation results. For the final set of simulations, a structured mesh including 768 elements in the pipe cross section is adopted (Figure 3). Being the simulations made in the time domain, physical quantities are

evaluated as a time average over an appropriate time interval after the reaching of steady-state conditions.

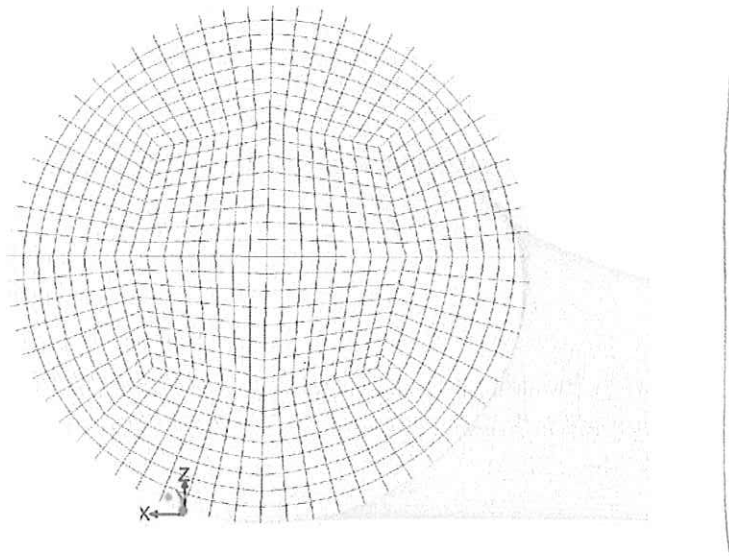


Figure 3 Computational grid used for the simulations.

4. Grid sensitivity study

Considering the 0.109 m diameter coil, three different flow conditions are simulated with three meshes, characterized by an increasing number of grid points. For every grid, the number of element in the axial direction has been determined to maintain as close as possible to 1 the aspect ratio of every hexahedral cell. The characteristics of the four grids and the conditions simulated are summarized in Table 2.

While the void fraction remains almost constant, the frictional pressure drop is considerably more influenced by the number of elements in the grid. The behaviour of the frictional pressure drop per unit length as a function of the number of grid elements is shown in Figure 4. Even if a grid independent solution is not obtained, the variation in the value of frictional pressure drop is included in the range 5-10 % doubling the number of elements in the mesh. As a further increase in the number of grid points results in an y^+ below the suggested working range of the wall function ($30 \leq y^+ \leq 300$), the mesh with 768 elements has been judged appropriate for the simulations. $\rightarrow \text{B}$

Table 2 Grid used and flow conditions simulated in the grid sensitivity study. The number of elements in each grid is indicated as number of elements in the tube cross section plus number of elements in the axial direction.

Mesh	n	n/V [m ⁻³]	Case	j _w [m/s]	j _a [m/s]	α _{in} [-]
1	192 x 100	2896	1	0.9	0.2	0.1
2	432 x 148	9643	2	0.8	0.6	0.2
3	768 x 200	23167	3	0.855	0.165	0.1

This
connect? or
with 0.16?

No
conclusions

3 diff mesh
3 diff flow condition

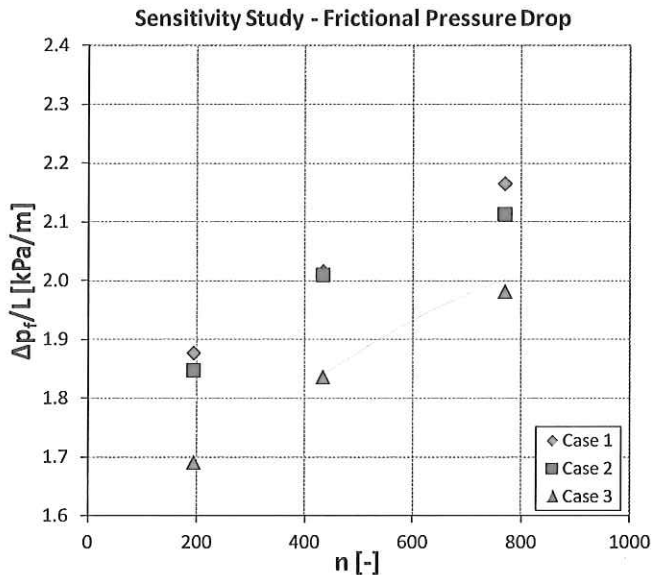


Figure 4 Behavior of the frictional pressure drop per unit length as a function of the number of elements in the computational grid.

5. Influence of the diameter of the dispersed phase

A large number of different parameters characterizes the CFD simulation of a two-phase flow, making it a very challenging subject. Amongst them, one of the most important and sensitive parameter has been recognized in the diameter of the dispersed phase (Krepper et al., 2008, 2013; Yun et al., 2012). As stated before, the code assumes the secondary phase to form droplets or bubbles and the diameter of the dispersed phase becomes the length scale to calculate the interaction between the phases. Bubble diameters are not available from experiments, neither are observation on the evolution of the bubble population. While this kind of data can be found in straight pipes (Lucas et al., 2005; Prasser et al., 2007), they are still missing for helical pipes. In particular, how the flow field produced by the centrifugal force affects the bubble population. Therefore, a sensitivity study on the value of the diameter of the dispersed phase has been carried out.

Case 1 of the grid sensitivity study (Table 2) was simulated also with different values of the dispersed phase diameter, ranging from 0.075 mm to 0.5 mm. Increasing the value of the bubble diameter, the average value of the void fraction in the channel cross section is reduced. Consequently, the slip ratio between the phases is increased, being constant the mass flow rate of the two phases. In Figure 5 and Figure 6, the void fraction on the pipe cross section is shown for a dispersed phase diameter equal to 0.1 mm and 0.2 mm, respectively. Although the average value is only slightly different, as the void fraction is reduced from $\alpha = 0.173$ to $\alpha = 0.169$, higher local differences are observed. In particular, a higher separation between the two phases appears as they flow along the channel. If the diameter is increased further, the separation between the two phases is almost complete and the void fraction results very low, so the frictional pressure drop. As an example, for d_p equal to 0.5 mm, the void fraction and the frictional pressure drop are respectively 0.080 and 1.25 kPa/m, with respect to 0.173 and 2.17 kPa/m found with $d_p = 0.1$ mm. At the same time, the simulations are characterized by convergence problems, oscillations and errors in the mass balance. Reducing the value of d_p to 0.075 mm, instead, does not alter significantly the results. A

d_p is not naturally imposed in CFD models, however it can be used as a threshold for bubble formation, drag increase etc.

further decrease, however, leads to an increase of both the void fraction and the frictional pressure drop. With a value of d_p sufficiently low, homogeneous flow conditions are reached. In other words, a higher diameter of the dispersed phase originates a weaker interaction between the two-phases, resulting in a clear separation between air and water, a higher value of the slip ratio and lower value of the void fraction. A reasonable value of the dispersed phase diameter was identified in $d_p = 0.1$ mm and maintained equal throughout all the simulations. The value of the diameter is lower if compared with typical air-water flow in straight pipes (Lucas et al., 2005; Prasser et al., 2007). This can be related to some deficiencies of the present model dealing with the physics of two-phase flow in helical pipes.

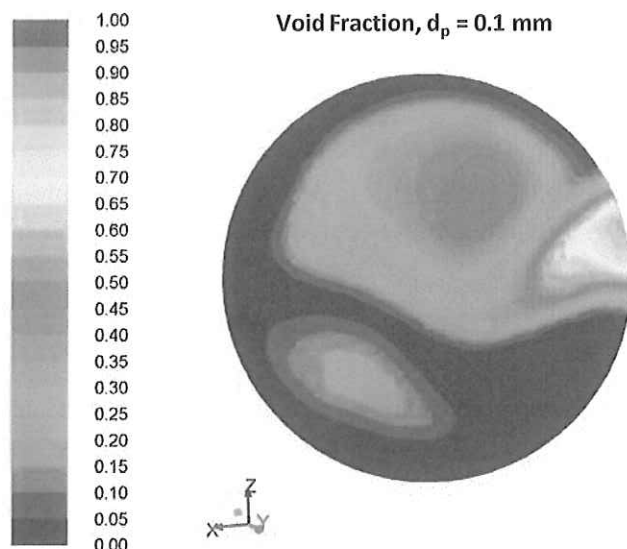


Figure 5 Void fraction obtained for $D = 0.109$ m, $j_w = 0.9$ m/s, $j_a = 0.2$ m/s and a diameter of the dispersed phase $d_p = 0.1$ mm.

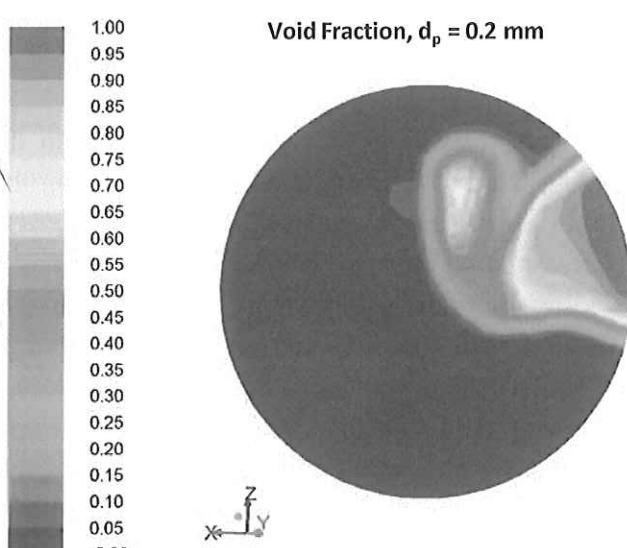
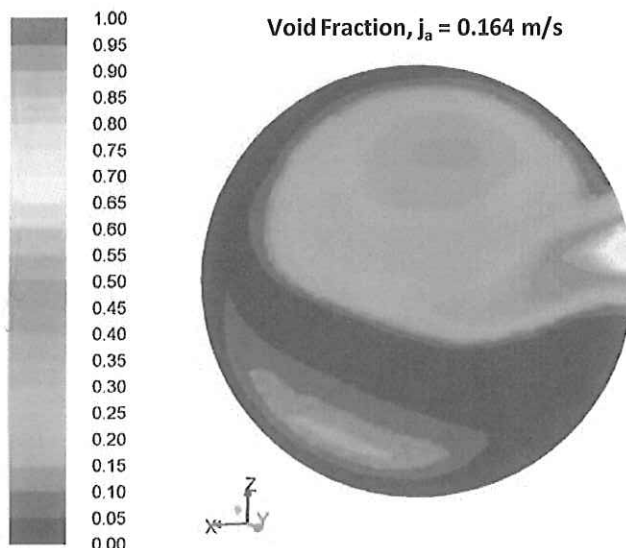


Figure 6 Void fraction obtained for $D = 0.109$ m, $j_w = 0.9$ m/s, $j_a = 0.2$ m/s and a diameter of the dispersed phase $d_p = 0.2$ mm.

6. Characterization of the air-water flow

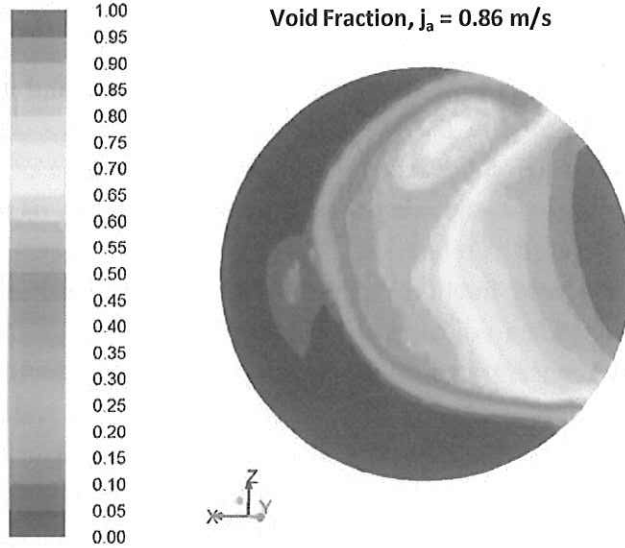
Three sets of experimental conditions were considered, at $j_w = 0.85 \text{ m/s}$ and $j_w = 1.16 \text{ m/s}$ for the $D = 0.109 \text{ m}$ coil and at $j_w = 0.35 \text{ m/s}$ for the $D = 0.225 \text{ m}$ coil. Numerous values of air superficial velocity j_a were simulated for each condition, to study the whole range of void fraction. In this section, the main characteristics of the air-water flow are depicted using CFD results. The simulations at $j_w = 0.85 \text{ m/s}$ are used as reference.

Figures from 7 to 9 show the void fraction profile and the phase distribution on the pipe cross section. For a very low value of the void fraction (Figure 7), the gravitational force is dominant, since the lighter air is mainly concentrated on the upper portion of the duct. Nevertheless, a slight effect of the centrifugal force field is already observable, as the heavier water tends to occupy the external section of the pipe, whereas the air accumulates near the internal wall. In addition, a water film at the wall and a recirculation pattern of the water phase are present in the upper portion of the duct, evidence of the presence of a secondary motion. As the air flow rate is increased, so the void fraction, the effect of the centrifugal force becomes clearer (Figure 8). The heavier water is pushed toward the outer wall of the tube, while the lighter air phase occupies the inner portion of the pipe, creating a highly unsymmetrical flow pattern in the radial direction. This phenomenon becomes more evident as the air flow rate is further increased, as shown in Figure 9.

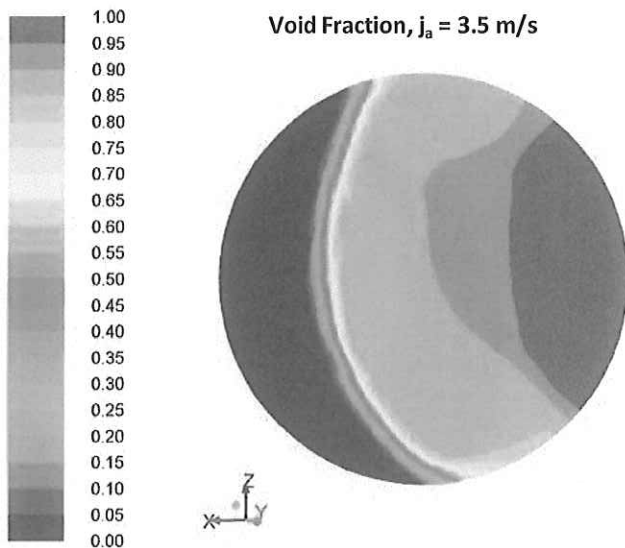


How is
centrifugal force
treated in
Fluent?

Figure 7 Profile of the void fraction on the tube cross section for $D = 0.109 \text{ m}$, $j_w = 0.85 \text{ m/s}$, $j_a = 0.164 \text{ m/s}$ and $\alpha = 0.155$.



20 Figure 8 Profile of the void fraction on the tube cross section for $D = 0.109 \text{ m}$, $j_w = 0.85 \text{ m/s}$, $j_a = 0.86 \text{ m/s}$ and $\alpha = 0.436$.
21
22
23
24



45 Figure 9 Profile of the void fraction on the tube cross section for $D = 0.109 \text{ m}$, $j_w = 0.85 \text{ m/s}$, $j_a = 3.5 \text{ m/s}$ and $\alpha = 0.680$.
46
47
48

49 The relative weight between centrifugal and gravitational force fields is also influenced by the
50 liquid superficial velocity. At the lowest value of the liquid superficial velocity ($j_w = 0.35 \text{ m/s}$), the
51 gravitational force remains dominant also for high values of void fraction and air superficial
52 velocity (Figure 10). On the contrary, at the highest value of the liquid superficial velocity ($j_w = 53$
54 1.16 m/s), the confinement of the water phase near the external pipe wall is even more evident
55 (Figure 11).
56

57 CFD results found confirmations with some visual observations obtained through imaging
58 tomography, available from the work of Murai et al. (2005). A good qualitative agreement is found
59 for the void fraction and the distribution of the phases. The latter preliminary confirms that the
60
61
62
63
64

rather simple CFD model adopted (only the drag force is considered for the interfacial momentum exchange between the phases) is able to reproduce the fundamental characteristics of the two-phase flow in the helical pipe. This suggests that is the centrifugal force that mainly influences the phase distribution and the interaction between the phases.

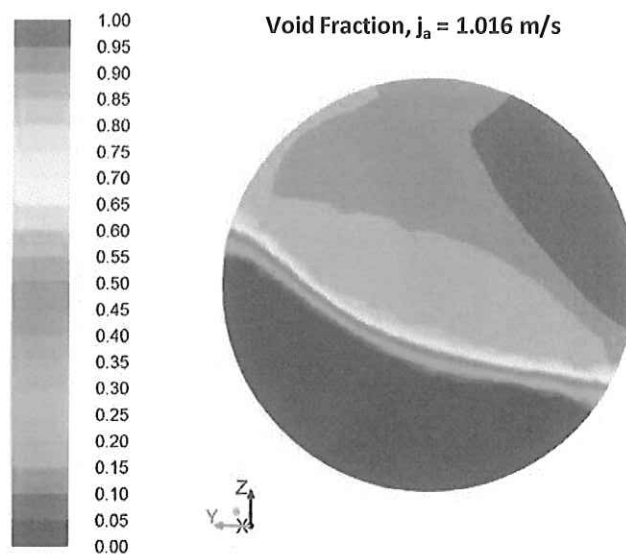


Figure 10 Profile of the void fraction on the tube cross section for $D = 0.225 \text{ m}$, $j_w = 0.85 \text{ m/s}$, $j_a = 1.016 \text{ m/s}$ and $\alpha = 0.612$.

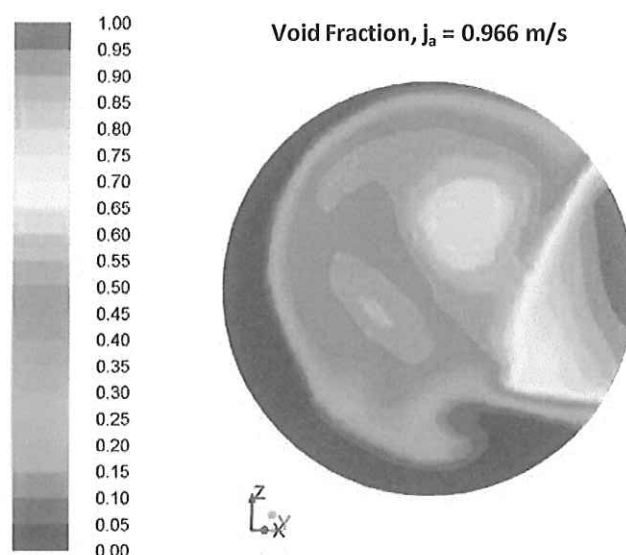


Figure 11 Profile of the void fraction on the tube cross section for $D = 0.109 \text{ m}$, $j_w = 1.16 \text{ m/s}$, $j_a = 0.966 \text{ m/s}$ and $\alpha = 0.417$.

Since the centrifugal force promotes a certain phase separation that increases with the void fraction, the velocity field reflects the particular phase distribution. The air, being the fluid with the lower density, flows with a higher velocity. In addition, the relative velocity between air and water is increased due to the high separation between them. As a consequence, the maximum of the velocity

ok ?? Why?

is shifted near the internal wall of the pipe, where the air accumulates under the effect of the centrifugal force field. On the opposite, the outer portion of the pipe becomes a low velocity region, being occupied by the water. This phenomenon becomes more and more evident as the air flow is gradually increased. In Figure 12, the velocity field is shown for $j_a = 1.25 \text{ m/s}$.

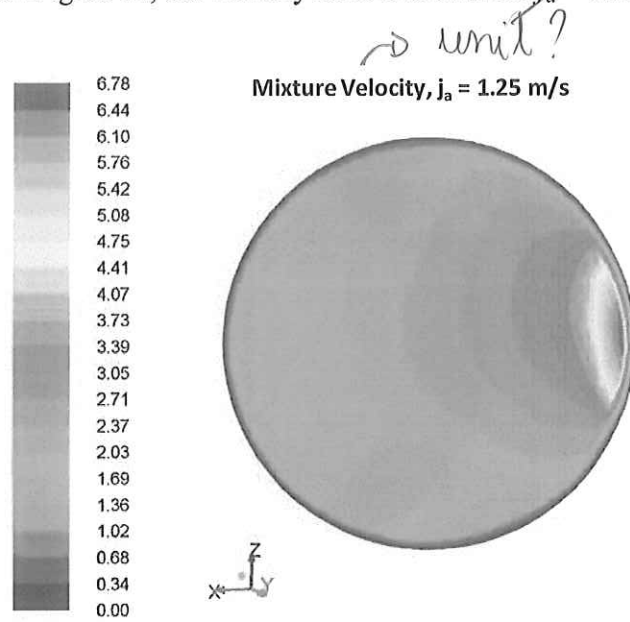


Figure 12 Profile of the mixture velocity on the tube cross section for $D = 0.109 \text{ m}$, $j_w = 0.85 \text{ m/s}$, $j_a = 1.25 \text{ m/s}$ and $\alpha = 0.497$.

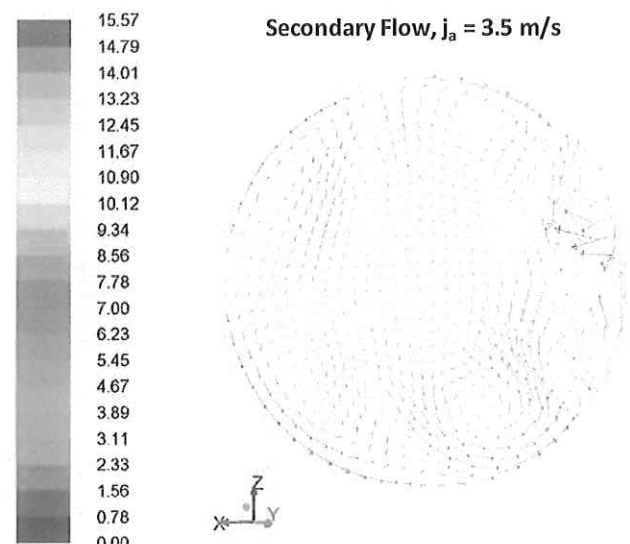


Figure 13 Secondary flow on the tube cross section for $D = 0.109 \text{ m}$, $j_w = 0.85 \text{ m/s}$, $j_a = 3.5 \text{ m/s}$ and $\alpha = 0.680$.

As in single-phase flow, the centrifugal field generates a secondary motion on the channel cross-section in the form of counter rotating vortices. Figure 13 illustrates this secondary motion. Two well defined, counter rotating vortices appear in the air region, together with other recirculation structures located in the maximum velocity region. The recirculation is maintained also inside the

phases

water, but the two vortices are confined toward the outside wall, being high the void fraction, so the volume occupied by the air phase.

7. Comparison with experiments

All the simulation results are presented in Table 3. A first comparison with the experimental data is shown in Figure 14 for the void fraction. The general agreement is good and the average relative error is about 4.5 % (Table 4). In more details, the largest errors are found for the two lowest void fractions, that are underestimated of more than 10 %. In particular, the lowest is underestimated of more than 15 %. Nevertheless, the absolute error remains very small and equal to about 0.03, being very small also the void fraction. At the same time, the higher error suggests a more complex behavior of the phase distribution at low flow quality. Therefore, a dedicated model of the drag force could be required to improve the accuracy of the simulations. The results of the previous section, indicating an interaction between the phases dominated by the centrifugal force, remain valid for higher void fraction, where the results are rather good. In particular, neglecting the points at $\alpha < 0.25$, the average relative error is reduced to 2.5 %, that can be considered inside the experimental uncertainty.

Table 3 CFD results in both simulated helical tubes ($D = 0.109 \text{ m}$ for $j_w = 0.85 \text{ m/s}$ and $j_w = 1.16 \text{ m/s}$ and $D = 0.225 \text{ m}$ for $j_w = 0.35 \text{ m/s}$).

$j_w [\text{m/s}]$	$j_a [\text{m/s}]$	x	α	$\Delta p/L [\text{kPa/m}]$
0.85	0.164	0.000235	0.155	2.038
0.85	0.86	0.001227	0.438	2.579
0.85	1.25	0.001791	0.500	2.871
0.85	1.97	0.002806	0.587	3.507
0.85	2.5	0.003551	0.627	3.953
0.85	3.0	0.004269	0.657	4.308
0.85	3.5	0.004984	0.680	4.598
1.16	0.380	0.0004	0.238	3.584
1.16	0.966	0.0010	0.433	4.999
1.16	1.500	0.0016	0.516	5.751
0.35	1.013	0.0035	0.612	0.820
0.35	4.451	0.0153	0.810	2.238

Table 4 Summary of the accuracy of the CFD simulations.

Conditions	α	$\Delta p/L$
$D = 0.109 \text{ m}, j_w = 0.85 \text{ m/s}$	4.5 %	15.2 %
$D = 0.109 \text{ m}, j_w = 1.16 \text{ m/s}$	4.8 %	6.3 %
$D = 0.109 \text{ m}, j_w = 0.35 \text{ m/s}$	2.0 %	13.0 %
Global	4.55 %	12.3 %

For the frictional pressure drop, the comparison is shown in Figure 15. For the data at $j_w = 0.85 \text{ m/s}$, the accuracy of the numerical results is high at low flow quality, but a systematic underestimation emerges starting from the medium flow quality. The average relative error is about 15 %, with maximum deviations included in the range $\pm 20 \text{ %}$. For the data at $j_w = 1.16 \text{ m/s}$, the average relative error is equal to 6.3 %, whereas it is about 13 % for the data at $j_w = 0.35 \text{ m/s}$. On the whole, an average relative error of 12.3 % is found for the frictional pressure drop (Table 4). Actually, the results can be considered satisfactory, as the errors are not significantly higher with respect to the

best literature correlations, when applied on their original databases. In Figure 15, the simulation results are compared to the correlations of Akagawa et al. (1971), which shows a great accuracy as expected. In addition, also the correlation from Xin et al. (1997), obtained from air-water data in helical coils, is added for comparison. Accuracy is high for the $D = 0.109$ m diameter coil, whereas greater errors are found for the $D = 0.225$ m coil. Being coil diameter critical for an accurate prediction of frictional pressure drop, a change in its value often determines the struggle of empirical correlations to predict experiments. For CFD results instead, the differences from the experimental data are almost comparable changing the flow conditions and the geometry of the coil using the same simulation parameters.

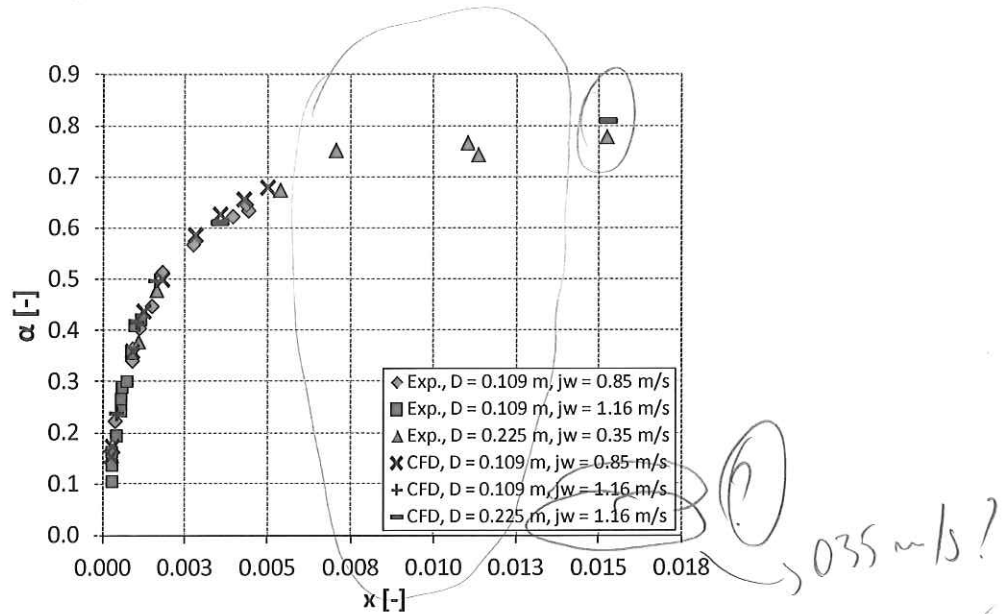


Figure 14 Comparison between the experimental data and the CFD results for the void fraction in all the simulated conditions.

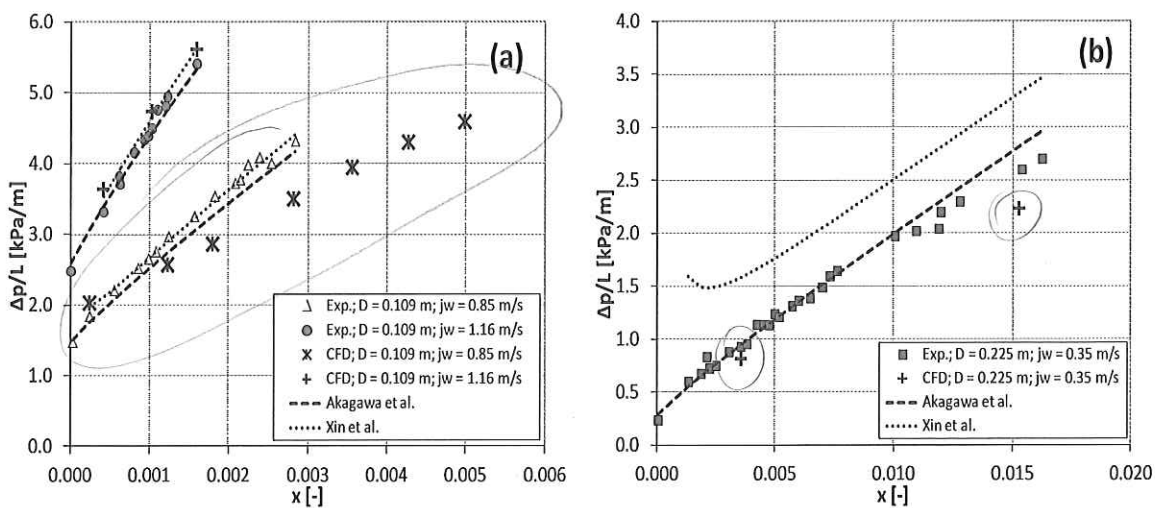


Figure 15 Comparison between the experimental data, CFD results and correlations by Akagawa et al. (1971) and Xin et al. (1997) for the frictional pressure drop. (a) $D = 0.109$ m, $j_w = 0.85$ m/s and $j_w = 1.16$ m/s. (b) $D = 0.225$ m and $j_w = 0.35$ m/s

flow refine?

Since the diameter of the dispersed phase has been identified as a critical parameter, some simulations ($D = 0.109$ m, $j_w = 0.85$ m/s) were repeated with a lower value of d_p . No differences were found for the void fraction, so results are shown in Figure 16 only for the frictional pressure drop. They are compared with the experimental data and the previous simulations. At low flow quality, no significant differences are found. At medium-high flow qualities, a higher value of the frictional pressure drop is generally obtained, closer to the experimental data. The average relative error becomes 8.2 % from the 15.2 % obtained with the higher value of the dispersed phase diameter. Although it is possible to further improve the simulation results with a fine tuning of the diameter of the dispersed phase, the above is out of the scope of this work, seeming also more related to a case by case scenario. Actually, the main objective is to demonstrate the possibility to estimate with a satisfactory degree of accuracy the void fraction and the frictional pressure drop in a wide range of conditions. As a consequence, no more work has been done to improve the results with a further tuning of the dispersed phase diameter.

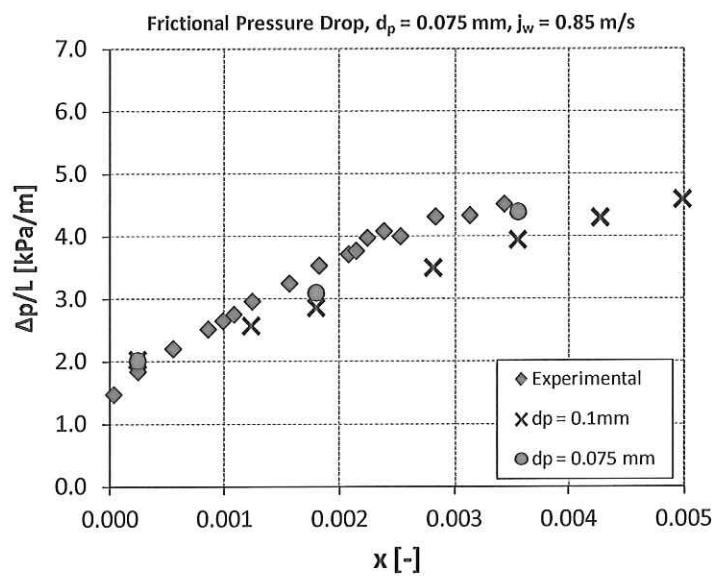


Figure 16 Comparison between the CFD results ($D = 0.109$ m and $j_w = 0.85$ m/s) and the experimental data for different values of the dispersed phase diameter d_p .

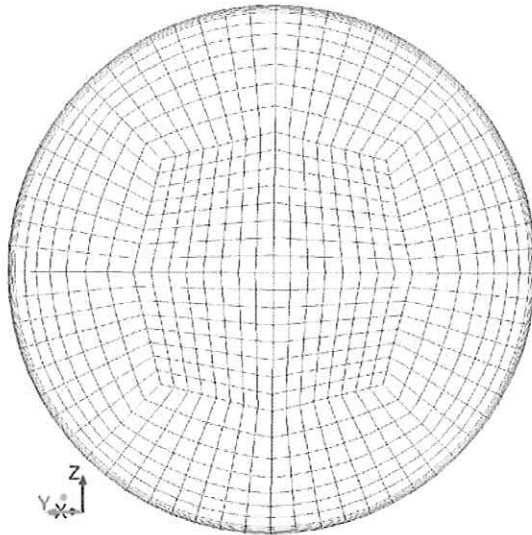
7.1. Effect of the wall treatment

Finally, also the influence on the results of the treatment of the near wall region has been examined. To the aim, the enhanced wall treatment of the ANSYS FLUENT code has been adopted. The enhanced wall treatment considers a two layer model in which the viscosity affected near wall region is resolved all the way to the viscous sub-layer (ANSYS FLUENT, 2011). Differently from wall function, no empirical formula is required to solve the region between the wall and the first grid point. First, since the enhanced wall treatment requires a sufficiently fine mesh, a new grid has been developed, introducing a finer boundary layer in the mesh of Figure 3. The new grid, composed by 1024 cells in the cross section, is shown in Figure 17. The same experimental points used in the previous section to quantify the effect of the dispersed phase diameter have been again simulated. Numerical results are resumed in Table 5.

Wall or exponential jd near the wall?

Table 5 Results of the simulation with the enhanced wall treatment.

j_w [m/s]	j_a [m/s]	x	α	$\Delta p/L$ [kPa/m]
0.856	0.161	0.0002	0.151	2.055
0.857	1.254	0.0018	0.501	3.671
0.860	2.486	0.0035	0.634	5.913



1
2
3
4
5
6
7
8
9
10
11
12
13
14
15
16
17
18
19
20
21
22
23
24
25
26
27
28
29
30
31
32
33
34
35
36
37
38
39
40
41
42
43
44
45
46
47
48
49
50
51
52
53
54
55
56
57
58
59
60
61
62
63
64
65

Figure 17 Computational grid developed for the simulations with the enhanced wall treatment.

The presence of the boundary layer allows a better definition of the phase distribution in the cross section of the pipe, in particular for the liquid film at the wall. Figure 18 show a comparison between the same experimental conditions simulated with the enhanced wall treatment and the wall function. For the major part, the results are unchanged. Instead, in the region occupied by the air-phase, a liquid film at the wall is present when the enhanced wall treatment is enabled. Actually, the enhanced wall treatment allows for a better definition of the wall region. In particular, the liquid film covers the majority of the wall and only the internal portion is excluded.

From a quantitative point of view, the average cross section values of the void fraction are unchanged with respect to previous results. The frictional pressure drop is well predicted until the medium values of the void fraction. However, it is significantly overestimated at high void fraction (Figure 19). Therefore, new simulations were made with a reduced dimension of the last cell near the wall. A slight improvement is shown at high void fraction. Nevertheless, the frictional pressure drop remains overestimated (Figure 19). Although it seems that a further reduction of the y^+ at the wall could lead to a further improvement of the results, no additional simulations were made. Actually, a reduction in the dimension of the last cell means an increase of the total number of grid cells, to maintain a reasonable ratio between the dimensions of consecutive elements. That is, a significant increase of the needed computational resources. In addition, the value of the y^+ in the latter simulations is already significantly low and equal to about 1.0 – 1.5.

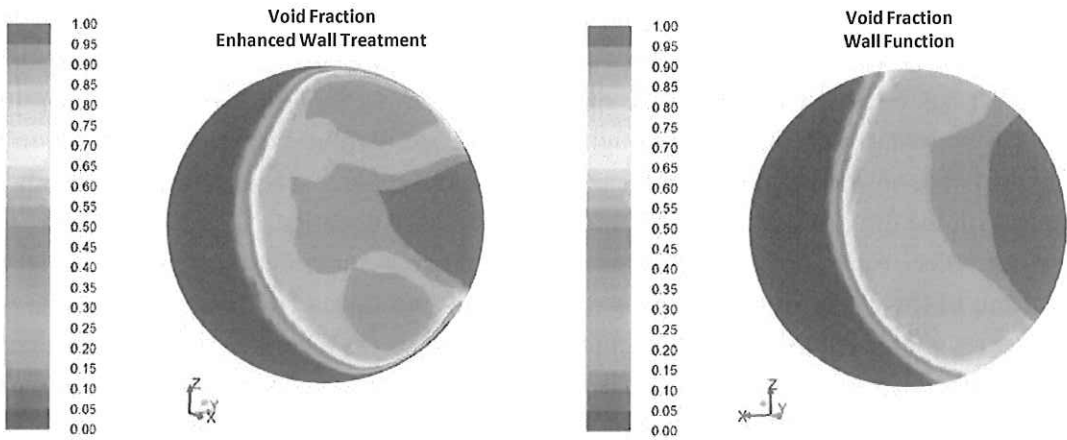


Figure 18 Profile of the void fraction on the tube cross section obtained using for the near wall region the enhanced wall treatment and the wall function respectively ($D = 0.109 \text{ m}$, $j_w = 0.85 \text{ m/s}$, $j_a = 2.5 \text{ m/s}$).

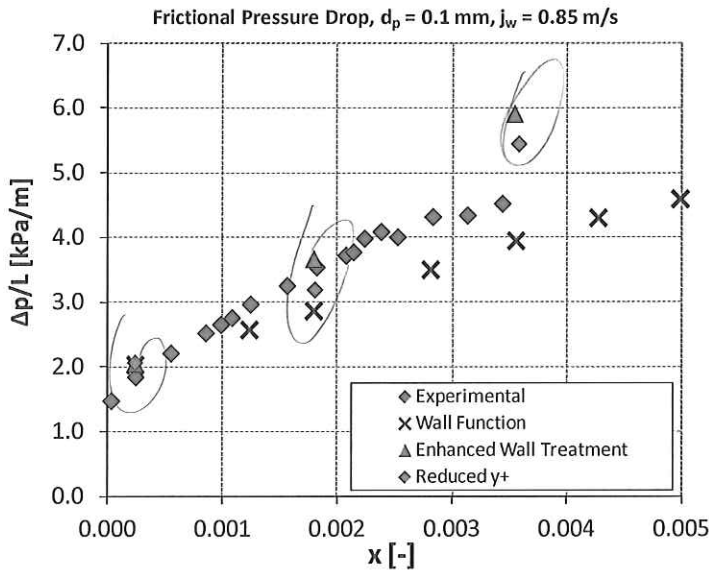


Figure 19 Comparison between CFD frictional pressure drop results obtained with the enhanced wall treatment and the wall function.

8. Conclusions

In this paper, a numerical study of two-phase air-water flow inside helically coiled pipes has been proposed. Attention to helical pipe thermal hydraulics within the nuclear field is stimulated by their expected employment for the SGs of different nuclear reactor projects of Generation III+ and Generation IV. In addition to the substantial improvement in heat and mass transfer rates and critical heat flux, their compact design is actually of interest for Small-medium Modular Reactors which adopt an integral design of the primary system. In this view, improvement of the general efficiency of the SG is expected to contribute reaching the goals of improved safety and economy established for future reactor projects. Although, the thermal hydraulic behavior of the helically coiled tube must be fully understood to contribute to the development of helical coil steam

generators. In addition, great benefit would come from availability of numerical tools giving reliable predictions of the physical quantities relevant for component design and safety operation. Therefore, CFD has been employed for the analysis. The ANSYS FLUENT code has been used, describing the two component mixture through the Eulerian-Eulerian model. An adiabatic mixture has been considered, neglecting heat transfer between the phases and accounting for the momentum transfer only with the drag force term in the momentum balance equation.

Simulations results were able to generate understanding providing a proper qualitative characterization of the effect of the centrifugal force field introduced by the geometry. The water, being the heavier phase, is pushed by the centrifugal force toward the outer pipe wall, whereas air accumulates in the inner region of the pipe. As a consequence, the maximum of the mixture velocity is found near the inner pipe wall, as the air flows much faster than the water, having a considerably lower density. The flow field, as for the single-phase flow, is characterized by flow recirculation and vortices. Confirmations to the CFD results were found in the work of Murata et al. (2006), which made available experimental observations of the phase distribution obtained through imaging tomography. As the value of the dispersed phase diameter is particularly important, its influence on the results has been studied. In particular, it defines the degree of interaction between the phases, passing from an excessive separation with a too high value to a homogeneous flow when the value falls under a certain threshold.

The data of Akagawa et al. (1971) allowed also a quantitative validation for the void fraction and the frictional pressure drop, relevant for the SG design. A good agreement was observed for the void fraction, with an average relative error of about 4.5 %. Since the model considers only the drag force but catches the fundamental features of the phase distribution, it seems mainly the centrifugal field that characterizes the interaction between the phases. However, at low void fraction, where also the gravitational force plays a significant role, errors are higher, suggesting the need of a more detailed modeling. A satisfactory estimation of the frictional pressure drop was also obtained, with an average relative error of 12.3 %. A comparison with two literature correlations showed a comparable accuracy. For one in particular, due to Xin et al. (1997), the error depends on the coil diameter, which often limits the range of applicability of empirical correlations. On the contrary, for the CFD model a comparable accuracy has been obtained in all flow conditions and coil geometries. In this view, the CFD model can be regarded has a reliable predictive tool that can help the safe design and the engineering analysis of helical pipe SGs to be employed in nuclear reactors.

Nomenclature

C_D	drag coefficient [-]
D	coil diameter [m]
d	tube diameter [m]
d_p	diameter of the dispersed phase [m]
f	drag function [-]
g	gravitational acceleration [m/s^2]
j	superficial velocity [m/s]
K	momentum interphase exchange coefficient [$\text{kg/m}^3\text{s}$]
L	length [m]
n	number of elements in the mesh [-]

1	p	pressure [Pa]
2	R	momentum interphase source term [$\text{kg}/\text{m}^2\text{s}^2$]
3	Re	Reynolds number [-]
4	T	stress tensor [Pa]
5	t	time [s]
6	V	volume [m^3]
7	v	velocity [m/s]
8	x	quality [-]
9	y^+	non-dimensional wall distance [-]
10		
11		
12		
13		
14		
15		
16		
17		Greek symbols
18		
19	α	void fraction [-]
20	μ	viscosity [Pa·s]
21	ρ	density [kg/m^3]
22	σ	surface tension [N/m]
23	τ	relaxation time [s]
24		
25		
26		
27		
28		Subscripts
29		
30	a	air
31	e	effective
32	in	inlet
33	w	water
34		
35		
36		
37		
38		References
39		
40		
41	B.K. Akagawa, T. Sakaguchi, M. Ueda, 1971. Study on a gas-liquid two-phase flow in helically coiled tubes. JSME Int. J. B-Fluid T. 14(72), 564-571.	
42		
43	N. Anderson, Y. Hassan, R. Schultz, 2009. Analysis of the hot gas flow in the outlet plenum of the very high temperature reactor using coupled RELAP5-3D system code and a CFD code. Nucl. Eng. Des. 238, 274-279.	
44		
45	ANSYS Fluent 14.0 User Guide, 2011.	
46	D.L. Aumiller, E.T. Tomlinson, W.L. Weaver, 2002. An integrated RELAP5-3D and multiphase CFD code system utilizing a semi-implicit coupling technique. Nucl. Eng. Des. 216, 77-87.	
47		
48	A. Bejan, A.D. Kraus, 2003. Heat Transfer Handbook. Wiley.	
49	D. Bertolotto, A. Manera, S. Frey, H.M. Prasser, R. Chawla, 2009. Single-phase mixing studies by means of a directly coupled CFD/system code tool. Ann. Nucl. Energy 36, 310-316.	
50		
51	D. Bestion, 2012. Applicability of two-phase CFD to nuclear reactor thermohydraulics and elaboration of Best Practice Guidelines. Nucl. Eng. Des. 253, 311-321.	
52		
53	A. Bousbia-Salah, F. D'Auria, 2007. Use of coupled code technique for Best Estimate safety analysis of nuclear power plants. Prog. Nucl. Energ. 49, 1-13.	
54		
55		
56		
57		
58		
59		
60		
61		
62		
63		
64		
65		

- T.T. Chandratilleke, N. Nadim, R. Narayanaswamy, 2012. An investigation of flow boiling with secondary flow interaction in curved pipes. ECI 8th International Conference on Boiling and Condensation Heat Transfer, Lausanne, Switzerland, 3-7 June.
- L. Cinotti, M. Bruzzone, N. Meda, G. Corsini, C. Lombardi, M. Ricotti, L. Conway, 2002. Steam generator of the International Reactor Innovative and Secure. Proceedings of the 10th Conference on Nuclear Engineering (ICON 10), Arlington, VA, USA, 14-18 April.
- V. Czop, D. Barbier, S. Dong, 1994. Pressure drop, void fraction and shear stress measurements in an adiabatic two-phase flow in a coiled tube. Nucl. Eng. Des. 149, 323-333.
- N.I. Kolev, 2005. Multiphase flow dynamics 2: thermal and mechanical interactions. Springer, Berlin, Germany, 2nd Edition.
- E. Krepper, D. Lucas, T. Frank, H.M. Prasser, P.J. Zwart, 2008. The inhomogeneous MUSIG model for the simulation of polydispersed flows. Nucl. Eng. Des. 238, 1690-1702.
- E. Krepper, R. Rzebak, C. Lifante, T. Frank, 2013. CFD for subcooled flow boiling: Coupling wall boiling and population balance models. Nucl. Eng. Des 255, 330-346.
- J.S. Jayakumar, S.M. Mahajani, J.C. Mandal, K.N. Iyer, P.K. Vijayan, 2010. Thermal hydraulic characteristics of air-water two-phase flows in helical pipes. Chem. Eng. Res. Des. 88, 501-512.
- J.C. Jo, W.S. Kim, C.Y. Choi, Y.K. Lee, 2009. Numerical simulation of subcooled flow boiling heat transfer in helical tubes. J. Press. Vess.-T. ASME 131.
- D. Lucas, E. Krepper, H.M. Prasser, 2005. Development of co-current air-water flow in a vertical pipe. Int. J. Multiphas. Flow 31, 1304-1328.
- S.N. Mandal, S.K. Das, 2003. Gas-liquid flow through helical coils in vertical orientation. Ind. Eng. Chem. Res. 42(14), 3487-3494.
- Y. Murai, H. Oiwa, T. Sasaki, K. Kondou, S. Yoshikawa, F. Yamamoto, 2005. Backlight imaging tomography for gas-liquid two-phase flow in a helically coiled tube. Meas. Sci. Technol. 16, 1459-1468.
- P. Naphon, S. Wongwises, 2006. A review of flow and heat transfer characteristics in curved tubes. Renew. Sust. Energ. Rev. 10, 463-490.
- S.V. Patankar, 1980. Numerical heat transfer and fluid flow. Hemisphere, Washington, DC, USA.
- H.M. Prasser, M. Beyer, H. Carl, S. Gregor, D. Lucas, H. Pietruske, P. Schutz, F.P. Weiss, 2007. Evolution of the structure of a gas-liquid two-phase flow in a large vertical pipe. Nucl. Eng. Des. 237, 1848-1861.
- A. Prosperetti, G. Tryggvason, 2007. Computational Methods for Multiphase Flow. Cambridge University Press, Cambridge, UK.
- M.R. Rahimi, A. Askari, M. Ghanbari, 2011. Simulation of two-phase flow and heat transfer in helical pipes. 2nd International Conference on Chemistry and Chemical Engineering IPCBEE, Singapore.
- S.Z. Rouhani, E. Axelsson, 1970. Calculation of void volume fraction in the sub cooled and quality boiling regions. Int. J. Heat Mass Tran. 13, 383-393.
- M. Santinello, 2012. Experimental and CFD investigations of single-phase and two-phase steam-water flow in helically coiled tubes. M.Sc. Thesis, Nuclear Engineering Division, Department of Energy, Politecnico di Milano, Milano, Italy.
- H.C. Unal, 1978. Determination of void fraction, incipient point of boiling, and initial point of net vapor generation in sodium-heated helically coiled steam generator tubes. Transaction of the ASME, J. Heat Tran. 100, 268-274.

- S. Vashisth, K.D.P. Nigam, 2009. Prediction of flow profiles and interfacial phenomena for two-phase flow in coiled tubes. *Chem. Eng. Process.* 48, 452-463.

O. Watanabe, O. Tajima, T. Nakano, M. Shimoya, 1986. Flow and heat transfer of a gas and liquid two-phase flow in helical coils. *JSME Int. J. B-Fluid T.* 54(507), 3192-3199.

M.A. Woldesemayat, A.J. Ghajar, 2007. Comparison of void fraction correlations for different flow patterns in horizontal and upward inclined pipes. *Int. J. Multiphas. Flow* 33, 347-370.

R.C. Xin, A. Awwad, Z.F. Dong, M.A. Ebadian, 1997. An experimental study of single-phase and two-phase flow pressure drop in annular helicoidal pipes. *Int. J. Heat Fluid Fl.* 18, 482-488.

B.J. Yun, A. Splawski, S. Lo, C.H. Song, 2012. Prediction of a subcooled boiling flow with advanced two-phase flow models. *Nucl. Eng. Des.* 253, 351-359.

N. Zuber, J.A. Findlay, 1965. Average volumetric concentration in two-phase flow systems. *J. Heat Tran.* 87, 453-468.

PE: Poor English. Authors should consider revise
the sentence(s).

SC: Sentence(s) is/are very confusing and do(es) not make any/much sense. Authors should revise it/them.

HIGHLIGHTS

- Eulerian multiphase model is applied to air-water flow inside helically coiled pipe
- Influence on the flow of centrifugal force introduced by geometry is characterized
- Numerical results are validated through comparison with experimental data
- Void fraction and frictional pressure drop are predicted with satisfactory accuracy
- CFD model is less limited in its range of applicability than available correlations